The impact of microstructural refinement on the tribological behavior of niobium processed by Indirect Extrusion Angular Pressing

Babak Omranpour Shahreza[1,2,3*], Marco A.L. Hernandez-Rodriguez[4], Edgar Garcia-Sanchez[4], Lembit Kommel[1], Fjodor Sergejev[1], Armando Salinas-Rodríguez[5], Anita Heczel[6,7], Jenő Gubicza[6]

1. Department of Mechanical and Industrial Engineering, Tallinn University of Technology (TalTech), Ehitajate tee 5, 12616 Tallinn, Estonia.
2. Hydrogen Research Institute, University of Quebec in Trois-Rivieres (UQTR), 3351 des Forges, Trois-Rivieres G9A 5H7, Canada.
3. Surface Engineering and Nanostructured Materials Research Group, Department of Chemical and Materials Engineering, Complutense University of Madrid (UCM), Av. Complutense, 28040 Madrid, Spain.
4. Facultad de Ingeniería Mécanica y Eléctrica (FIME), Universidad Autónoma de Nuevo León (UANL), 66455 San Nicolás de los Garza, Mexico.
5. Centro de Investigación y de Estudios Avanzados del Instituto Politécnico Nacional, Unidad Saltillo, Parque Industrial Saltillo, Ramos Arizpe 25900, Coahuila, Mexico.
6. Department of Materials Physics, Eötvös Loránd University (ELTE), Budapest, P.O.B. 32, H-1518, Hungary.
7. Department of Metallurgical and Materials Engineering, The University of Alabama, Tuscaloosa, AL 35487-0202, USA.

* Corresponding author; email address: omranpou@uqtr.ca

Abstract

This research, for the first time, conducted a comprehensive study into the effect of a modern Severe Plastic Deformation technique, "Indirect Extrusion Angular Pressing (IEAP)", on the microstructural refinement of niobium and the subsequent impact on the tribological properties. The samples were processed for 4, 9, and 12 passes of IEAP and then exposed to Pin-on-disk wear test in dry sliding conditions. The results showed that the grain refinement occurred in niobium from an average grain size of 13 μm to 0.5 μm, along with an increase in hardness from the initial value of 79 HV to 180 HV after 12 passes. Results of wear tests revealed that IEAP processing reduced the wear width, volume loss, and specific wear rate by 14%, 38%, and 38%, respectively, and thereby enhancing the wear resistance of the material. Evaluation of the morphology of wear tracks demonstrated less spalling and less fatigue propagated cracks as well as finer detachment of wear debris on the surface of the processed samples, which led to producing a mild wear regime. The outcomes suggested that IEAP processing resulted in higher resistance in niobium against abrasion and against the development of fatigue propagated cracks which were respectively associated with higher hardness and larger fractions of high-angle grain boundaries (HAGBs).

Keywords: Severe Plastic Deformation; wear; Microhardness; Scanning Electron Microscopy

1. Introduction

Niobium as a refractory-transition metal serves in different industrial and medical applications. As a hypoallergenic metal, it has been employed in jewelry and coin manufacturing technologies [1]. As a light-ductile metal, it has a wide range of applications in superconducting radio frequency (SCRF) technology [2,3], nuclear reactors, chemical processes [4], energy storage [5–7], cutting tool substrate in the form of carbide [8], etc. Niobium is usually covered with a dense layer of oxide, thereby providing a high level of corrosion resistance. The elongation of more than 20% and the low brittle-to-ductile fracture temperature of -125 °C make niobium very ductile and suitable for large deformations. As a refractory metal, the melting point (T_m) is quite high (2477

°C), implying a very high recrystallization temperature (~826 °C, which is approximately 40% of T_m in Kelvin degrees). These facts allow niobium to be utilized in Severe Plastic Deformations (SPD) without incurring the risk of fracture or dynamic recrystallization [9]. Nowadays, a systematic approach has been adopted to enhance the properties of metallic materials by means of grain refinement via SPD techniques [10]. This enhancement by grain refinement may contain different aspects in materials properties. The most important aspects are the improvement in mechanical properties [11–13], electrical properties [14–16], hydrogen sorption kinetics [7,17,18], corrosion resistance [19–21], biocompatibility [22,23], and wear resistance [24–27]. The wear and tribological behavior of materials are important aspects when designing structural parts that are in contact with each other because the wear of a machine element leads to increased clearance and loss of precision [28]. Earlier investigations performed on the SPD processing of niobium showed that grain refinement had a great impact on increasing the mechanical strength of the material [4,9,29–32]. One major aspect of strength is the resistance of materials against wear. A wide range of studies attempted to assess the impacts of SPD on the wear and tribological properties of different materials such as aluminum [33–36], tantalum [37], titanium [38,39], copper [40], etc. Nonetheless, the outcomes are controversial as they report that the wear resistance could decrease, increase, or remain unaffected after processing [41]. From the theoretical point of view, harder materials shall be more resistant against the abrasion of the counterpart surface in a tribosystem. The conventional equation of Archard (Equation 1) explicitly links the two parameters of wear and hardness [41]. This equation shows that volume loss of materials is inversely proportional to the hardness:

$$V_L = K \; \frac{LN}{H} \; ; \tag{1}$$

where V_L is the volume loss, K is the friction coefficient, L is the total sliding distance, N is the applied normal load, and H is the hardness of the material. The contradiction between the hardness increase and wear-resistance decrease was explained in light of the complexity of the wear mechanisms that contributed to the wear in the tribosystem [42]. It is generally accepted that wear is not the property of the materials; instead, it is the response of a tribosystem to the contact stresses. Therefore, several contributing factors may affect the wear, and no unique model is applicable to all situations [41].

Fatigue behavior of SPD-induced niobium has also absorbed the attention in the literature. It was revealed that ultra-fine grained (UFG) niobium alloy (Nb -1wt.% Zr) after SPD processing presented a stable cyclic deformation response compared to the coarse grain (CG) conditions as a result of microstructural evolution of niobium and the increased fractions of high angle grain boundaries (HAGBs) [43].

This work aims to study the impact of grain refinement on the tribological properties of a niobium alloy processed by a modern SPD technique. A modified Equal Channel Angular Pressing (ECAP) is exploited in this work for SPD processing and grain refinement of materials. ECAP is believed to be the most used of all SPD techniques [10]. The modified Indirect Extrusion ECAP die called Indirect Extrusion Angular Pressing (IEAP) was designed and employed in the experiments for the microstructural refinement with the main advantage of reducing the friction between the die

and workpiece during the process as compared to the conventional ECAP dies. Based on the traditional equation of strain in ECAP [44], this die imposes an equivalent Von Mises strain value of $\varepsilon \approx 1.155$ on the materials in each pass of extrusion. More details about the die geometry and indirect extrusion method of ECAP can be found elsewhere [45]. This type of ECAP die is helpful for processing high-strength materials, particularly at higher passes of extrusions when the strength of materials increases dramatically and thereby, increasing the risk of damaging the die or the punch [46,47]. In this work, niobium alloy with a purity of 98.5 wt.% was processed using the IEAP die. This material, as mentioned above, has great potential as a biomaterial thanks to its biocompatibility and inert nature, although with the main drawback in poor mechanical properties. Enhancing the mechanical and tribological properties of niobium, therefore, may arouse strong interest in the implementation of this material for biomedical applications [48].

2. Material and methods

2.1 Processing of materials

The Indirect Extrusion ECAP die (IEAP - shown in Figure 1) with a squared cross-sectional channel, a channel angle of $\phi = 90°$ and a corner angle of $\psi = 0°$, processed the materials using route B_c.
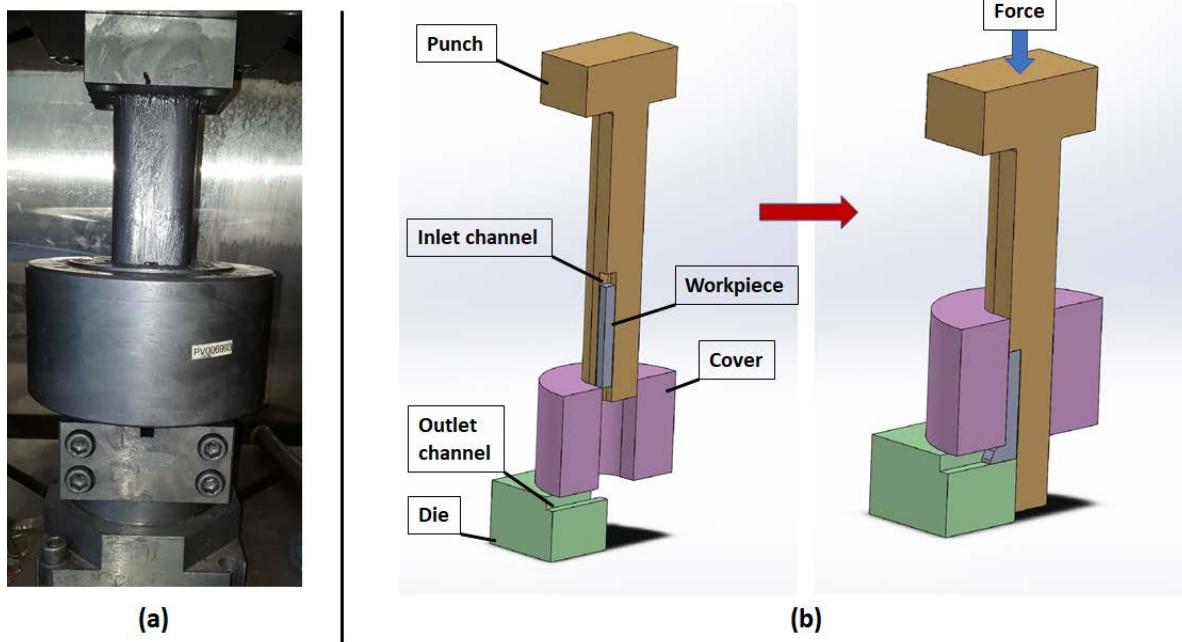

Figure 1: Indirect extrusion ECAP (IEAP); a): Die assembly; b): Schematic cross section of the die and the progress of the punch movement during deformation.

A dilute niobium (Nb) alloy with the chemical composition of Nb $\geq$ 98.5, Y $\leq$ 0.8, Ni $\leq$ 0.5, Ta $\leq$ 0.1 in wt.% provided by Neo Performance Materials (NPM) Silmet A.S. - Estonia, was received

as ingots and prepared with the dimension of 12×12×130 mm for IEAP processing. All IEAP experiments were conducted at room temperature and processed via route Bc where each sample rotated on its longitudinal axis between consecutive passes by 90 degrees in the same direction [49]. This route is expected to produce the most effective grain refinement with homogeneous microstructure and optimum superplastic ductility [44]. Molybdenum disulfide (MoS_2) was used as a lubricant during the extrusion. Niobium samples were processed for four, nine, and twelve passes of ECAP. A SHIMADZU HMV microhardness tester measured the hardness of specimens in the scale of Vickers (HV) with an applied load of 200 g for 15 sec. At least ten points were measured along the diameter of each specimen, and the average value was considered as the overall value of hardness.

2.2 Wear tests

All processed and initial billets were sectioned in a transversal direction and cut into smaller disks. Then they were mechanically polished up to 4000 grit sandpapers and then finely polished with suspensions of highly concentrated diamond with 3 and 1 μm particles, then cleaned with acetone and dried with hot air before the wear tests. A pin-on-disk tribometer equipped with a stereoscope and a digital camera, a load cell for recording the friction force, and a computer to process and compile the data were implemented in the experiments. The wear tests were performed in dry sliding conditions at the relative humidity of ~45%, the ambient temperature of 23 °C, and repeated three times for each sample. Redhill® Stainless steel bearing balls AISI 304 with a diameter of ø=11.1 mm, a surface hardness of 25 – 39 HRC, and surface roughness of $R_a = 0.5$ μm were employed as counterpart surface for pin-on-disk tests. The pin was fixed in the load arm and positioned perpendicular to the specimen. Rotating the specimen under the pin made a circular wear track with a diameter of 10 mm. Wear tests were conducted with a rotational speed of ω=200 ± 5 rpm. Accordingly, a relative sliding velocity of ~0.1 m/sec was achieved between the pin and disk. The wear tests were conducted with time steps of 30, 120, 300, 900, 1800, and 3000 sec on each sample which corresponds to the sliding distance of 3.14, 12.56, 31.4, 94.2, 188.4, and 314 m, respectively. A new pin was used in each experiment, and a load of 1 kg was applied vertically to the pin during the test. The mean and maximum values of Hertzian contact pressures were 0.49 and 0.73 GPa in this tribosystem. A non-contact 3D profiler (Carl Zeiss Axio CSM-700 confocal microscope) with a vertical resolution of 0.01nm and a lateral resolution of 0.38μm was employed to measure the volume loss and wear rate of the wear tracks. Six sections from each wear track with the dimensions of 320×1300 μm were measured by the profilometer, and then, the total volume loss was calculated based on the length of the wear track. All wear tests were performed in accordance with ASTM-G99 standards [50].

2.3 Material characterization

The morphology of worn surfaces was examined by using an Optical and a Scanning Electron Microscope (Nikon Epiphot 200 and a Hitachi SU8020, respectively). Analysis of the chemical composition of worn surfaces was conducted by using energy-dispersive X-ray (EDAX) spectroscopy running at 20 kV in the same electron microscope. The EBSD maps were taken by using an FEI Quanta 3D scanning electron microscope operating at 20 kV. The step size varied between 150 and 30 nm depending on the dimensions of the images. Orientation Imaging

Microscopy (OIM) software was used for the analysis of the EBSD results. A 15° criterion was employed to differentiate between the low-angle boundaries (LAGBs) and high-angle boundaries (HAGBs). In order to prepare the samples for EBSD measurement, the surfaces were mechanically polished up to 4000 grit SiC abrasive papers and then polished with 5, 3, and 1 μm aluminum oxide suspensions. The final step was accomplished by polishing the surface with a 40 nm colloidal silica suspension.

The lattice defect structure in the specimens was studied by X-ray line profile analysis (XLPA). The X-ray line profiles were measured by a high-resolution rotating anode diffractometer (RA-MultiMax9, manufacturer: Rigaku, Japan) using $CuK\alpha_1$ (wavelength, λ=0.15406 nm) radiation. Two-dimensional imaging plates detected the Debye-Scherrer diffraction rings. The peak profiles were evaluated by the convolutional multiple whole profile (CMWP) fitting procedure [51,52]. Using the CMWP method, the diffraction pattern is fitted by the sum of a background spline and the theoretical line profiles related to crystallite size and dislocations. For each reflection, the theoretical line profile was obtained based on the convolution of the theoretical size and strain profiles. The area-weighted mean crystallite size ($<x>_{area}$) and the dislocation density (ρ) were determined by the CMWP fitting evaluation procedure of the diffraction patterns. The value of $<x>_{area}$ is calculated as $<x>_{area}$=m·exp($2.5\sigma^2$), where m is the median and σ is the square root of the lognormal variance of the crystallite size distribution [51]. In the CMWP evaluation method, one fitting parameter is $C_{h00}b^2\rho$, where b is the modulus of the Burgers vector of dislocations and C_{h00} is the dislocation contrast factor for reflections with the indices *h00* (*h* is an arbitrary integer number). The Burgers vector for body-centered cubic (bcc) crystal structures is given as *a/2<111>*, where *a* is the lattice constant and equals 0.3306 nm. Accordingly, *b* equals 0.2863 nm for Nb alloys. The average contrast factors for reflections can be calculated numerically from the anisotropic elastic constants of the crystal [53]. The values of the elastic constants c_{11}, c_{12}, and c_{44} are 246.5, 134.5, and 28.7 GPa, respectively, for Nb alloys [54]. Using program ANIZC [55], the values of $\overline{C}_{h00}$ for the edge and screw dislocations were calculated as 0.119 and 0.165, respectively.

3 Results:
3.1 Evolution of the microstructure and mechanical properties
3.1.1 X-ray line profile analysis

Using the average contrast factors and utilizing the CMWP method, the crystallite size and the dislocation density were determined by fitting the calculated theoretical patterns to the experimental diffractograms. Figure 2 illustrates a CMWP fitting in logarithmic intensity scale for the sample deformed by 12 passes of IEAP. The crystallite size and the dislocation density are listed in Table 1. It is noted that the crystallite size obtained by XLPA in plastically deformed metallic materials is usually smaller than the grain size determined by electron microscopy. This difference can be explained by the fact that the crystallite is equivalent to the volume scattering X-rays coherently, and dislocation patterns inside the grains may break the coherency of X-rays. The present investigation shows that the crystallite size decreased while the dislocation density increased with the number of IEAP passes.
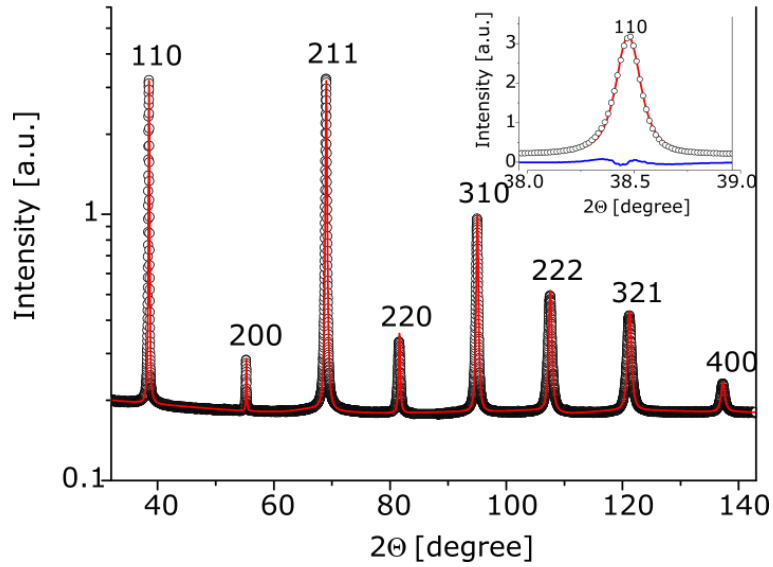
Figure 2: The CMWP fitting after 12 IEAP passes. The open circles and the solid line represent the measured data and the fitted curve, respectively. A part of the pattern is presented in the inset with a linear scale. The difference between the measured and the fitted patterns is shown at the bottom of the inset.

3.1.2 EBSD analysis and microhardness testing

Figure 3 shows the orientation distribution (left) and grain maps (right) for the initial and IEAP-processed specimens obtained by EBSD. The grains were defined as the volumes bounded by high-angle grain boundaries (HAGBs) with the misorientation angles higher than 15°. The average grain size in the initial sample with CG microstructure (~13 μm) was consistently refined to approach a UFG microstructure. This reduction of the grains size was down to ~ 4, 1.2, and 0.5 μm in the IEAP samples after 4, 9, and 12 passes, respectively.
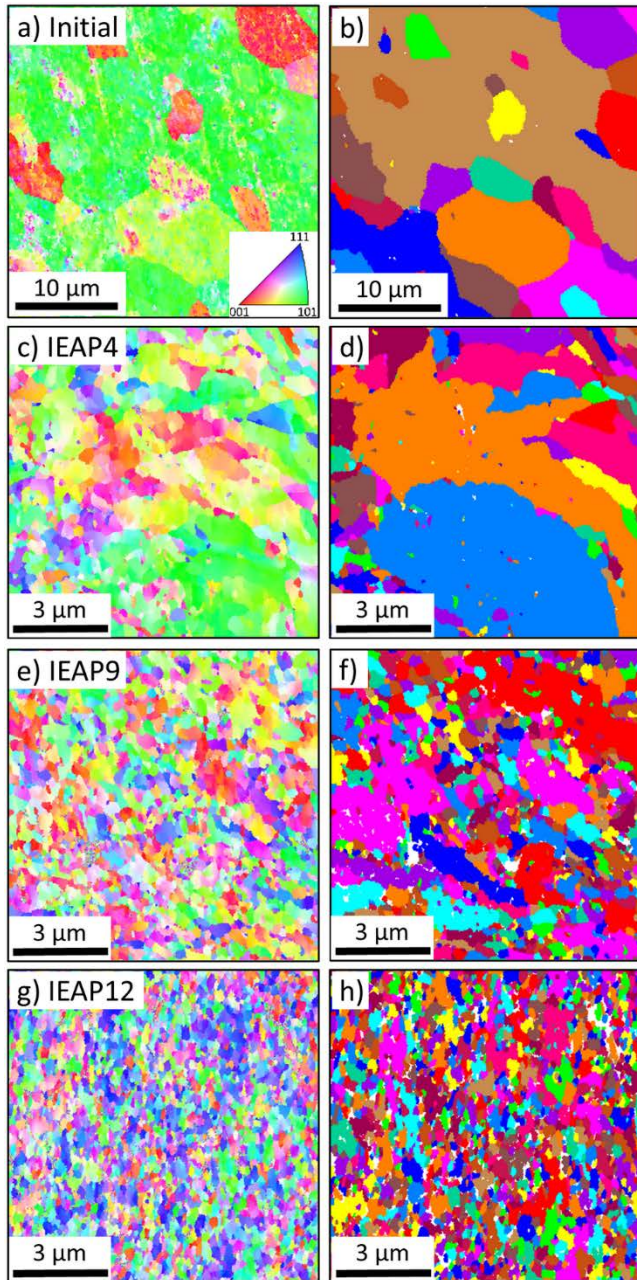
Figure 3: EBSD analysis of niobium demonstrating the orientation distribution (a,c,e,g) and the grain maps (b,d,f,h) in the initial specimen (a,b), and the processed specimens for 4 (c,d), 9 (e,f) and 12 (g,h) passes of IEAP.

The grain size- and misorientation angle- distribution in the samples are shown in Figure 4. As shown below, IEAP processing was able to increase the density of HAGBs in the material successively.
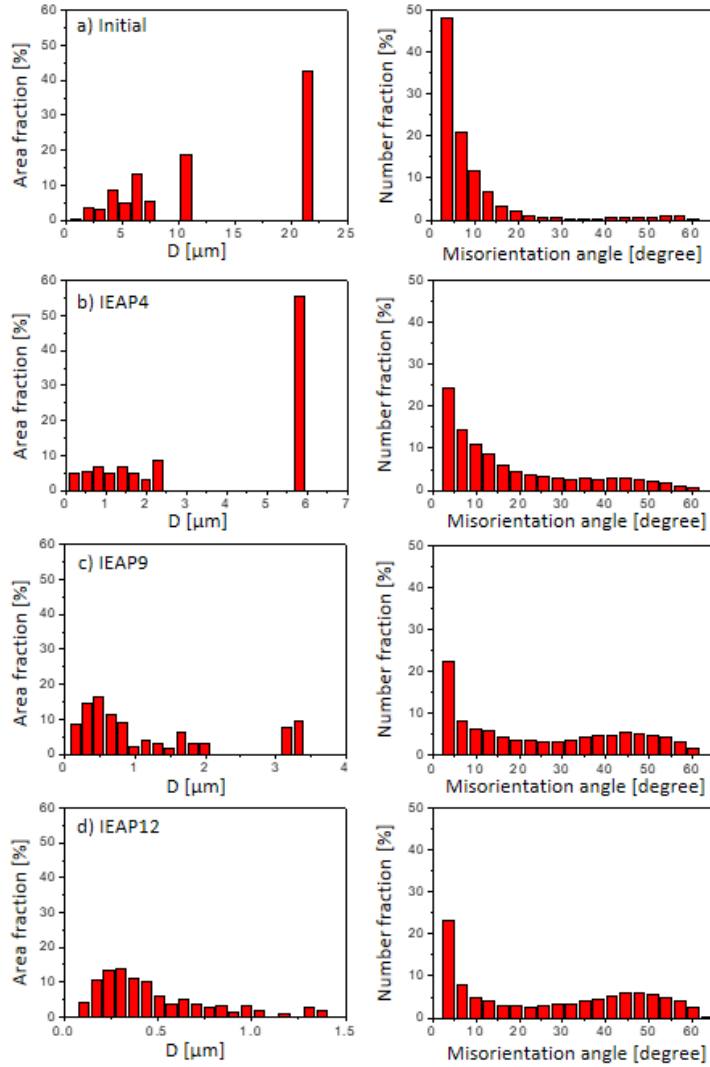
Figure 4: Distribution of the grain size (left) and the grain-boundary misorientation angles (right) in the initial sample (a), and the processed specimens after 4 (b), 9 (c), and 12 (d) passes of IEAP.

Structural parameters of the materials, including the mean value of grain size, crystallite size, dislocation densities, the fraction of high-angle grain boundaries as well as microhardness, and the equivalent strain imposed on the material, are given in Table 1. According to the results, the grain size significantly reduced after processing, and the hardness substantially increased. The rate of increase in hardness is appreciable at the early stages of IEAP extrusion (104% increase after four passes of IEAP). In comparison, this rate slightly decreased by the pass numbers (123% increase after twelve passes). A similar trend can be found in increasing the fraction of high-angle grain boundaries in the processed samples when compared to the initial one.

Table 1: Structural parameters of the initial and processed samples after IEAP. The area-weighted mean grain size (D_{area}) and the high angle grain boundary fraction ($V_{HAG\ B}$) were determined by EBSD; the area-weighted mean crystallite size ($<x>_{area}$) and the dislocation density (ρ) were obtained by XLPA, and the microhardness values were measured in Vickers scale.

Sample	Von mises strain	Microhardness [HV0.2]	D_{area} [μm]	$<x>_{area}$ [nm]	ρ [10^{14} m^{-2}]	V_{HAGB} [%]
Initial	-	79 ± 3	13 ± 2	-	-	20
IEAP 4	4.62	161 ± 4	3.9 ± 0.6	146 ± 18	3.0 ± 0.4	44
IEAP 9	10.39	177 ± 6	1.2 ± 0.2	97 ± 10	13 ± 2	58
IEAP 12	13.86	180 ± 4	0.5 ± 0.1	71 ± 8	16 ± 3	61

3.2 Wear test:

3.2.1   Coefficient of friction and wear rate

Evaluation of the coefficient of friction (CoF) in all samples did not present any noticeable change in values before and after IEAP processing. CoF in all samples ranged between ~0.30 to ~0.35, as shown in Figure 5.
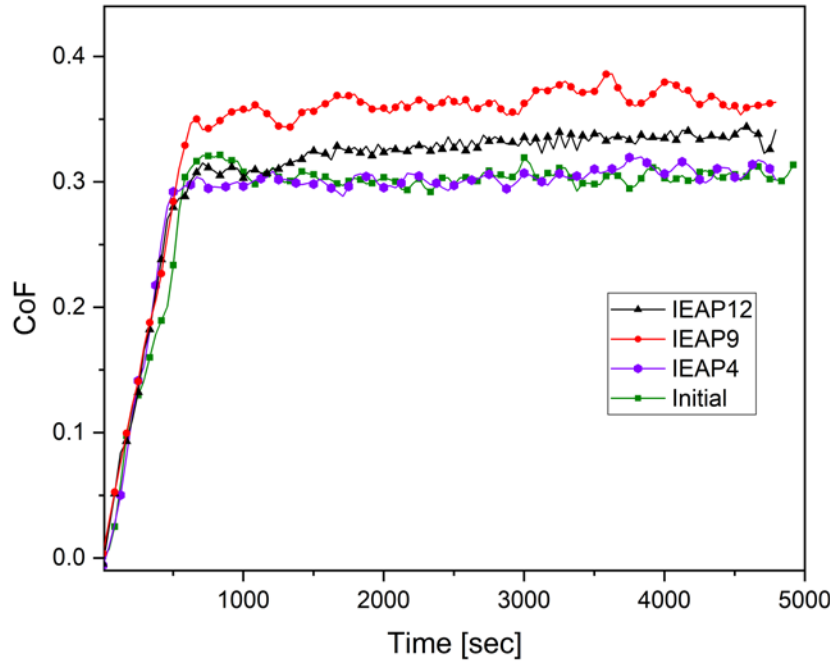

Figure 5: Demonstration of CoF with respect to the time in the initial and IEAP processed samples. The uncertainty is less than 7%.

Figure 6-a shows the volume loss (V_L) of the wear tracks obtained from the wear test. Figure 6-b represents the specific wear rate (W_s) based on the volume loss (V_L) per distance (L) per applied load (F_p): $W_s = V_L/(L \cdot F_p)$ [56].
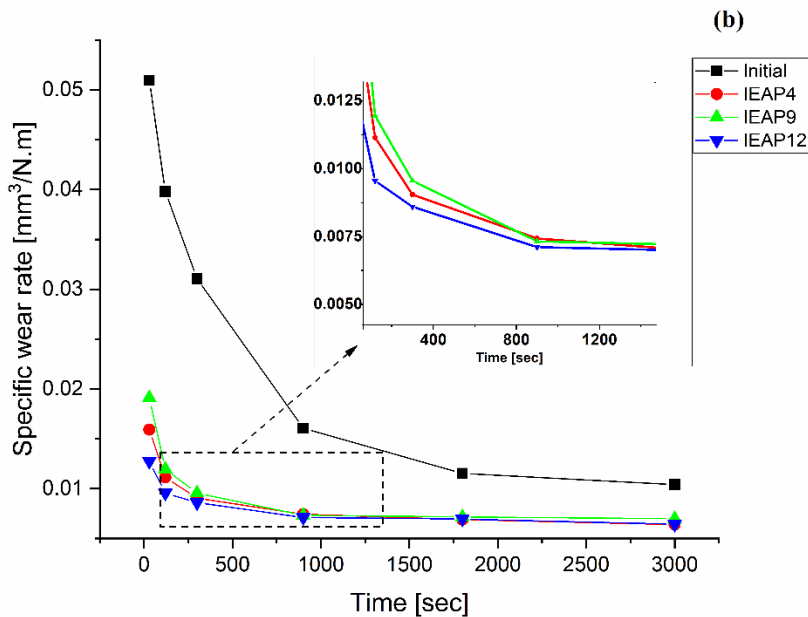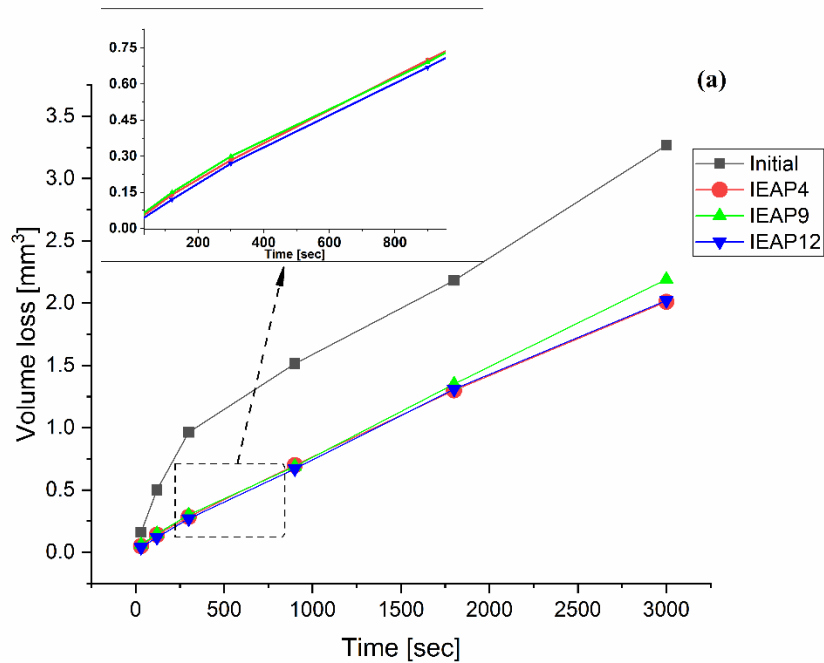
Figure 6: Effect of IEAP on the wear behavior of niobium;(a) Volume loss in the samples versus time; the inset graph shows the selected area with higher magnification of the volume loss with two decimal digits. (b) Specific wear rate versus time; the inset graph depicts the selected area of the wear rate with three decimal digits. The uncertainty is less than 12%.

These graphs show that applying IEAP and the subsequent grain refinement in the niobium samples decreased the volume loss and the wear rate down to 38%, but the number of extrusions had no significant influence on these parameters as the graphs for IEAP4, IEAP9, and IEAP12 overlapped each other. It is noticeable that the wear rate in the CG niobium was much higher at the beginning of the test (~4 times higher than that of UFG samples), and this trend changed and decreased at the steady-state zone, but still higher than the processed ones.

In order to better analyze the transition of the wear mechanisms during the test, optical microscopy of the wear tracks from the beginning of the test to the end within different time steps is provided in Figure 7, and the results of measurement of the width of wear tracks in the samples are collected in Figure 8. This graph is consistent with that of the volume loss and the wear rate illustrated earlier in Figure 6 since the corresponding values in all IEAP-processed samples overlapped each other. According to the results, the width at the steady-state conditions decreased down to ~14% after processing.
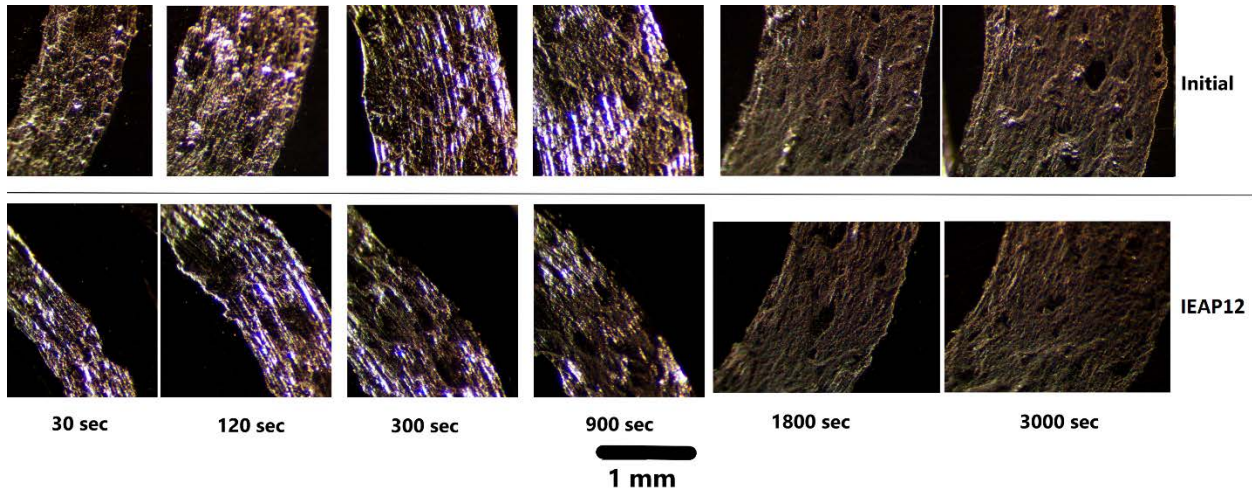

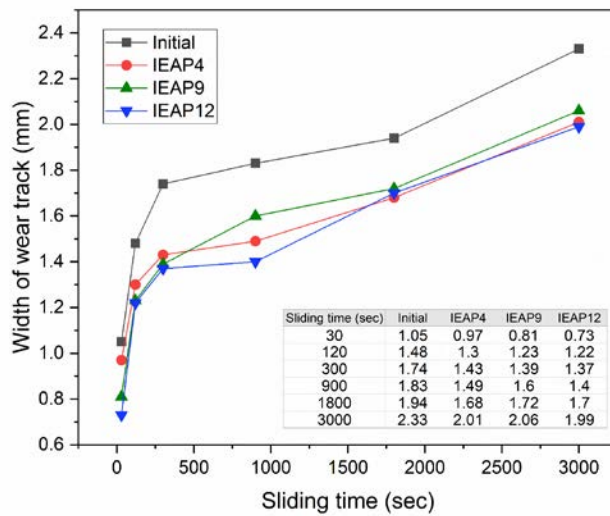Figure 7:Transition of the wear tracks by increasing the sliding time; images were obtained by optical microscopy.

| Sliding time (sec)	Initial	IEAP4	IEAP9	IEAP12
30	1.05	0.97	0.81	0.73
120	1.48	1.3	1.23	1.22
300	1.74	1.43	1.39	1.37
900	1.83	1.49	1.6	1.4
1800	1.94	1.68	1.72	1.7
3000	2.33	2.01	2.06	1.99

Figure 8: Evolution of the width of the wear track with respect to the sliding time. The width values presented here are the mean values of six sections of each wear track. The uncertainty is less than 10%.

3.2.2   Morphology of the wear tracks

SEM observations of the surface of wear tracks are presented in Figure 9. These images show the wear mechanisms of abrasion, adhesion, fatigue wear, and oxidation on the surface of the wear tracks in dry sliding conditions.
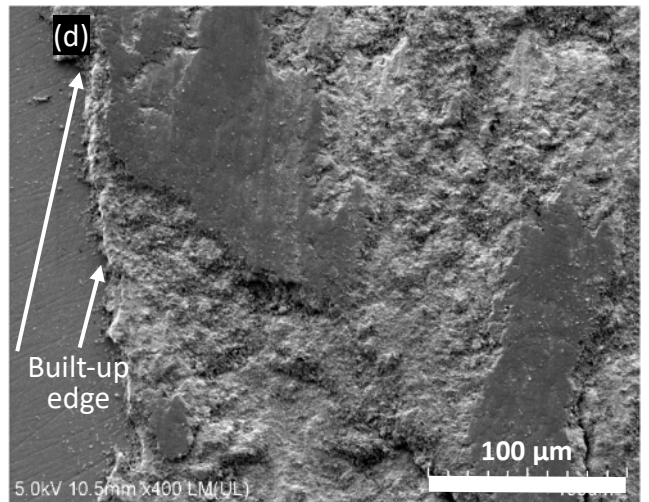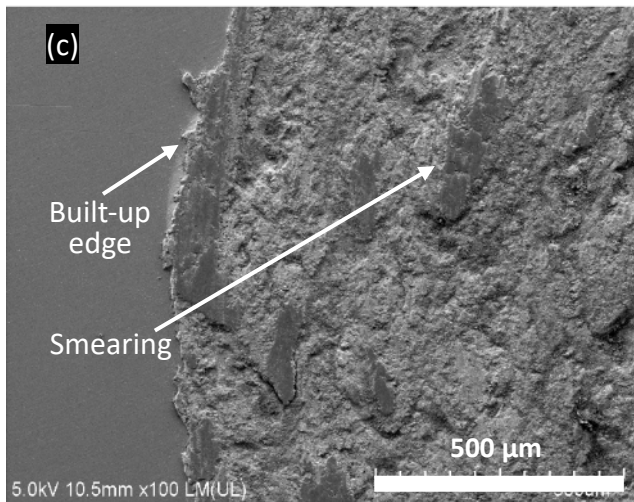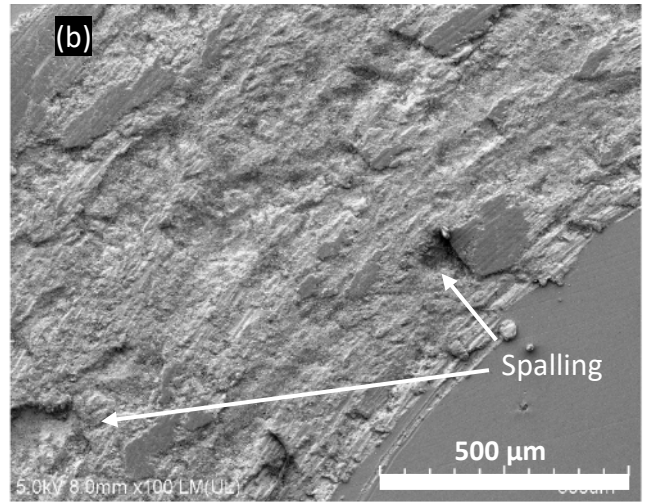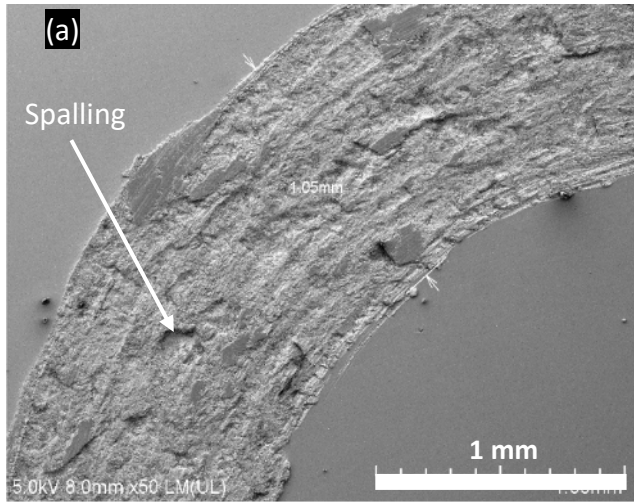
Figure 9: SEM images of the surface of wear tracks: Images obtained from the initial specimen with CG microstructure (a, b, c, and d); and the ones obtained from the IEAP12 specimen with UFG microstructure (e, f, g, and h).

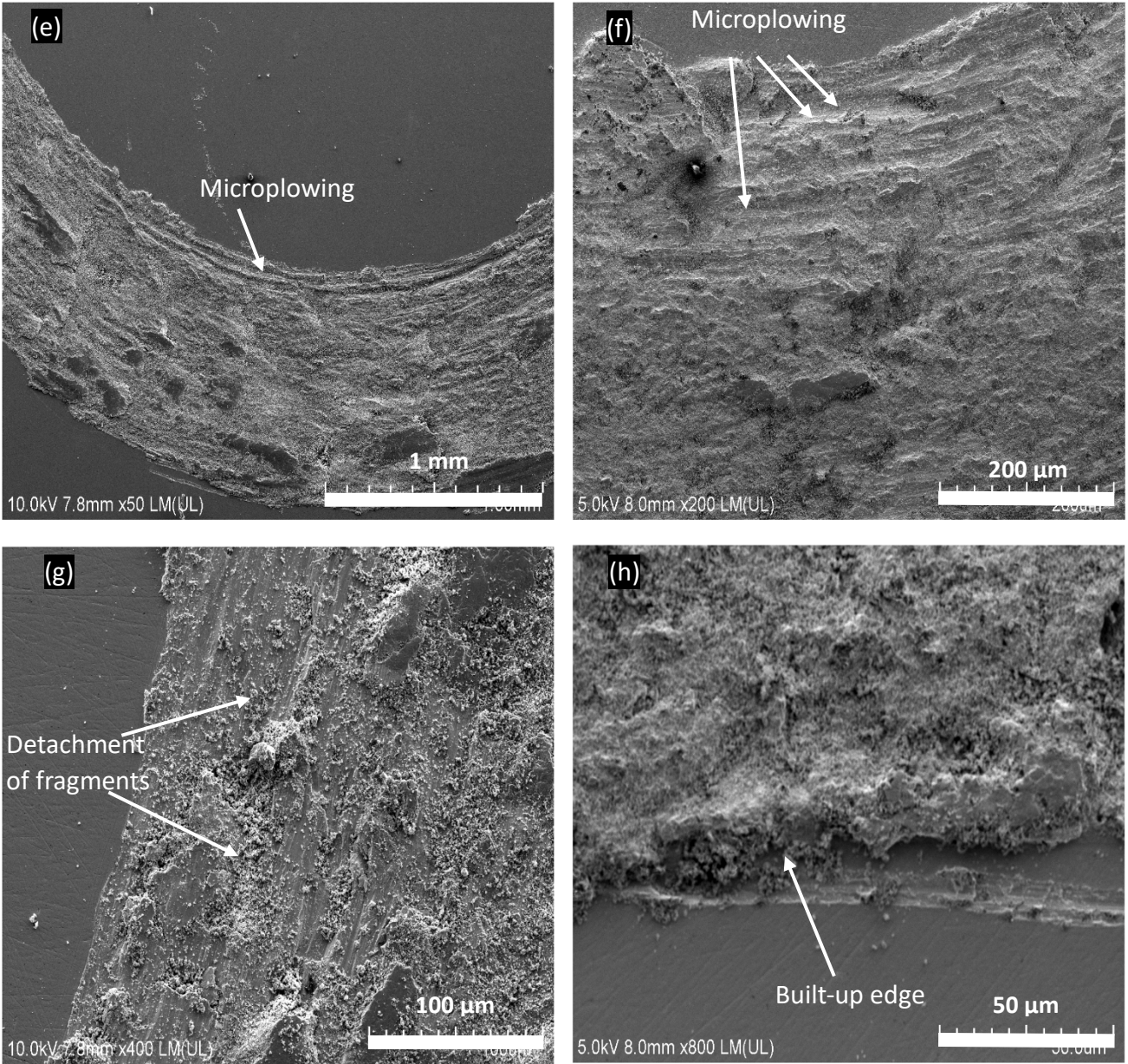The two mechanisms of abrasive and adhesive wear are predominant in both cases of CG- and UFG- microstructure by considering the evidence of microplowing and plastic deformations, the presence of ridges and grooves, as well as the formation of build-up edges and smearing of materials on the surface. In addition, EDX analysis of the wear tracks in the initial- and IEAP12- samples (shown in Figure 10) confirmed the appearance of oxidative wear. The results of EDX analysis are collected in Table 2. These results also imply the occurrence of materials transfer from the pin to the rotating disk in light of the presence of iron (Fe) and chromium (Cr) on the wear tracks.
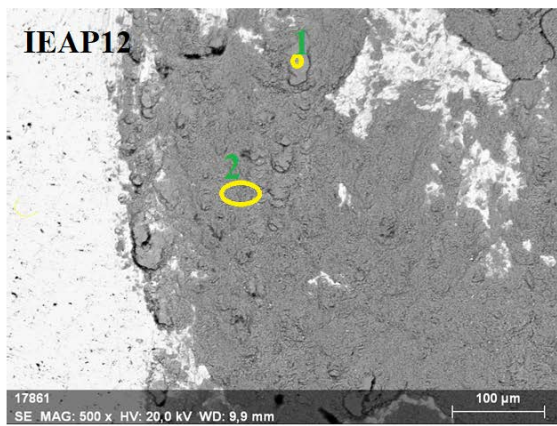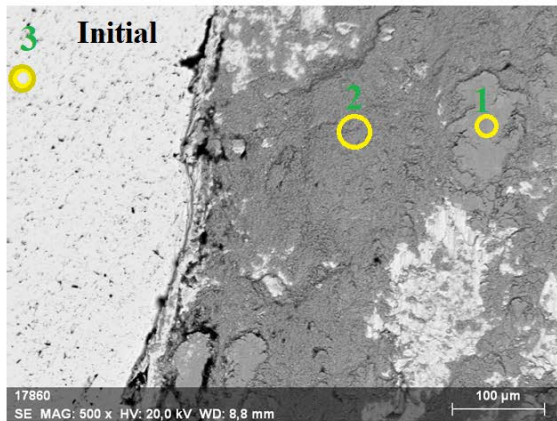
Figure 10: Demonstration of the selected areas used for SEM-EDX analysis.

Table 2: Results of EDX analysis of the processed (IEAP12) and unprocessed (Initial) samples

Sample		unn. C [wt.%]				
		Niobium	Oxygen	Iron	Chromium	Yttrium
Initial	Spectrum 1	68.34	22.84	3.71	1.61	0.51
	Spectrum 2	69.79	23.37	2.94	1.11	0.50
	Spectrum 3	92.62	5.35	-	-	0.70
IEAP12	Spectrum 1	64.14	27.23	3.15	1.55	0.67
	Spectrum 2	63.64	28.14	3.11	1.47	0.69

Another wear mechanism that is mainly found in the initial sample (CG microstructure) is the spalling of the surface as a result of fatigue wear. This type of wear results from repetitive strains imposed by sliding, succeeding to the crack development, separation of deformed materials, and eventually forming the spalls on the surface [58]; see Figure 9.

The other mechanism of the wear which is primarily discernible in the processed samples is the detachment of small fragments by plastic shearing. In macroscopic scales, fragmentation is a result

of brittle fracture appearing in brittle materials (as opposed to smearing in soft or ductile metals [57]. In this work, such fragmentations mark out the effect of work hardening and the reduction of ductility after IEAP processing. Indeed, imposing strains by IEAP and accumulation of dislocations in materials leads to increasing the hardness and hence, transitioning the wear mechanism to a mild form of wear in the processed samples.

4   Discussion

This research was meant to explore the evolution of microstructure and the possible impacts on the mechanical and tribological properties of a dilute niobium alloy by using a modern SPD technique called IEAP. SPD techniques such as ECAP and HPT were successfully employed in the literature to improve the mechanical properties of pure Nb by decreasing the grain size and increasing the dislocation densities; it was proved that dislocation density has a significant impact on the strength [29–31]. In this study, the dislocation density in niobium considerably increased by IEAP processing between 4 to 12 passes from $\sim 3 \times 10^{14}$ to $\sim 16 \times 10^{14}$ m^{-2}, while the crystallite size decreased from ~ 146 to ~ 71 nm. In a former study, the microstructural evolution in pure Nb during HPT-processing was investigated by XLPA, and it was shown that dislocation density increased to 80×10^{14} m^{-2} by increasing the equivalent strain up to 44 [30]. In the present work, the highest dislocation density ($\sim 16 \times 10^{14}$ m^{-2}) was measured after 12 passes of IEAP, which corresponds to the equivalent strain of 13.86. For HPT-processed Nb, the dislocation density was significantly higher, $\sim 60 \times 10^{14}$ m^{-2}, in a similar equivalent strain. In another study, the microstructure of pure Nb was investigated after different levels of deformation imparted by ECAP and HPT [29], and it was revealed that HPT fabricated slightly finer microstructures than ECAP at the same equivalent strain level. It should be noted that different processing parameters such as pressure could result in different microstructures at the same equivalent strain imposed by SPD; this fact could also explain the difference in dislocation densities at the same equivalent strain. Indeed, the higher pressure applied by HPT can hinder the diffusion, which is necessary for the annihilation of edge dislocations during SPD processing, thereby leading to the further accumulation of dislocations as compared to the case of IEAP.

According to the EBSD orientation maps (Figure 3), the average grain size of the initial Nb sample was refined after four passes of IEAP from ~ 13 to ~ 4 μm; the processed sample contains refined and coarse grains with the sizes between ~ 0.2 and ~ 5 μm. After nine passes of IEAP, the overall structure is more uniform, and the grain size varies between ~ 0.15 and ~ 3 μm. Further grain refinement was observed by increasing the IEAP passes up to twelve, and the average grain size reached the submicron scale (~ 0.5 μm). This investigation is in agreement with an earlier study where ECAP was applied to pure Nb, and for the initial state, the grain size varied between 20 - 40 μm [31]. After sixteen passes of ECAP, the average grain size was refined to ~ 0.4 μm, and in this study, a similar refinement was achieved after twelve passes of IEAP. Then, it could be concluded that the increased hardness by increasing the strain is closely connected to the increase in the dislocation densities and the decrease in the grain size.

A detailed inspection of the hardness and structural parameters of the material (Table 1), including the mean grain size and the fraction of HAGBs, shows that these parameters approach a saturation level by increasing the number of extrusions in IEAP (see Figure 11).
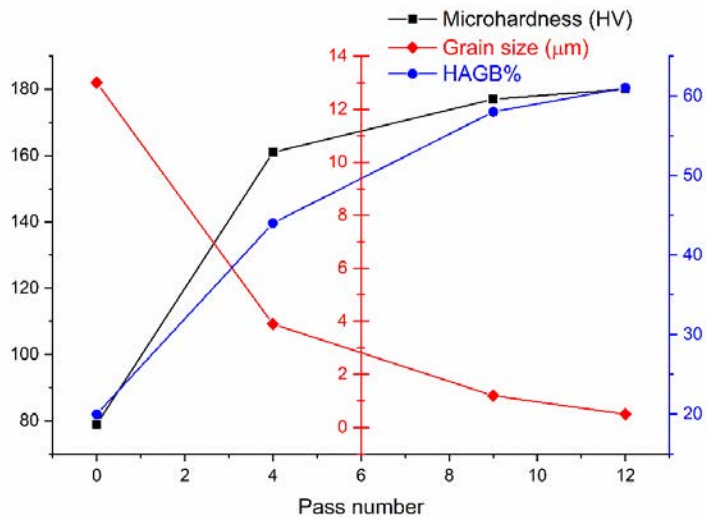
Figure 11: Illustration of the trend of saturation in structural parameters of the material depicted in a multi-layer graph: microhardness in black, the grain size in red, and HAGB fractions in blue. The 0th pass in the X-axis refers to the initial case.

Studies in the literature also suggest a similar trend of saturation in microstructural parameters and hardness after the grain refinement of niobium by ECAP [32,59–61]. However, a study about ECAP processing of commercially pure (CP) niobium with the purity of 99.7% processed up to 24 passes claimed that despite reaching the saturation in grain size after 4 to 8 passes, the HAGB fractions did not approach the saturation level [9]. This statement was challenged in another study on the processing of CP niobium (99.9%) with two different SPD techniques, ECAP and HPT [59]. This research showed that the saturation of structural parameters was not achieved by ECAP. At the same time, HPT and the combination of HPT and ECAP allowed the hardness and the microstructural features (including HAGBs) to approach a saturation stage. HPT has been widely used as a powerful SPD tool for microstructural refinement of metals and alloys owing to its capability to induce extremely large deformations in materials. This technique has two advantages over ECAP: 1) HPT can impose large amounts of strains, in the order of $\varepsilon = 100\text{-}500$, while strain values of 18 to 20 are quite high in ECAP. 2) HPT can exert high values of pressures in the order of 2-6 GPa to the material, whereas this number is in the order of hundreds of MPa for ECAP. This high level of pressure results in difficult recovery of dislocations and thus, further strengthens the material [59]. Even HPTE, a new generation of HPT which is able to produce bulk samples, has been proved to be capable of increasing the microhardness and grain refinement to higher levels along with a higher saturation hardness in CP aluminum (AA1050) when compared to those of ECAP [62]. Aside from the type of processing, the processing temperature is a key factor in governing the saturation of microstructural features. An investigation on the HPT processing of niobium at room- and cryogenic- temperatures elaborated on this fact [32] and showed that saturation was achieved at room-temperature processing, and any further deformation did not refine the microstructure because of reaching an equilibrium state in the generation and annihilation of defects as a result of dynamic recovery. On the other hand, it was disclosed that cryogenic processing of niobium retarded the saturation and helped to attain higher strength. However, what is important to point out here is that saturation in microhardness and

microstructural features in single-phase materials are affected by several parameters, of which the most important controlling factors are processing temperature, impurities, and alloying elements [63].

Results of the dry sliding wear test showed that IEAP processing of the samples decreased the volume loss and thus, reduced the wear rate (see Figure 6). This enhancement in the reduction of the wear rate, however, is only discernible between the initial and IEAP processed samples, and no significant change can be found among the processed samples with respect to increasing the number of extrusions. It is openly admitted that wear starts with the abrasion of the surface at the beginning of dry sliding wear tests [57]. As indicated earlier, hard materials are expected to be more resistant against abrasion; therefore, the processed samples with higher hardness presented more resistance against the wear (lower volume loss and wear rate). This fact is easily observable in Figure 7 at the beginning of the test ($t \approx 30$ sec), where IEAP12 possesses a narrower wear track. Increasing the sliding time and hence, the sliding distance of the ball on the disk results in the delamination, plastic deformation, as well as smearing of the materials leading to developing the other wear mechanisms comprised of adhesion and fatigue. In addition, the temperature of the contact surface increases and thereby intensifies the oxidative wear. As a result, introducing several factors in the tribosystem arises the complexity of the wear and dilutes the impact of hardness among the processed samples. Moreover, it should be noted that increasing the pass numbers of IEAP and imposing more strains reduces the ductility and decreases the strain-hardening capability [33,64], the two critical factors that are believed to be responsible for lowering the wear resistance of alloys in SPD processing [41].

The improved wear resistance of the IEAP-processed niobium as compared to the initial material, as indicated, is attributed to the increased hardness as a result of grain refinement and increased dislocation density (see Table 1). On the other hand, the increase of IEAP passes from 4 to 12 yielded only marginal improvement in the hardness and the wear rate despite the significant grain refinement and the rise of the dislocation density. Between 9 and 12 passes, although the dislocation density and the HAGB fraction remained practically unchanged, the grain size was further refined from 1.2 to 0.5 μm without any significant change in the hardness and the wear resistance. This apparent contradiction can be explained by the additional strain hardening resulting from both hardness and wear testing. For instance, hardness testing yields a plastic strain of about 8% during the pressing of the indenter into the surface of the material. This additional strain can harden the material. Since less deformed materials have higher strain hardening capability, the hardening caused by hardness testing is higher at lower numbers of IEAP passes. This effect can cause similar hardness values even if the microstructural features are different between 4 and 12 IEAP passes. The same can be applied for wear testing.

One noticeable difference in the morphology of the UFG and CG niobium samples is the appearance of several spalls as a result of fatigue wear on the surface of the CG niobium (see Figure 12), which resulted in the occurrence of severe wear and thus a higher volume loss. In comparison, the IEAP12 specimen (see Figure 9) and other UFG samples (not shown here) presented mild wear in the wear tests.
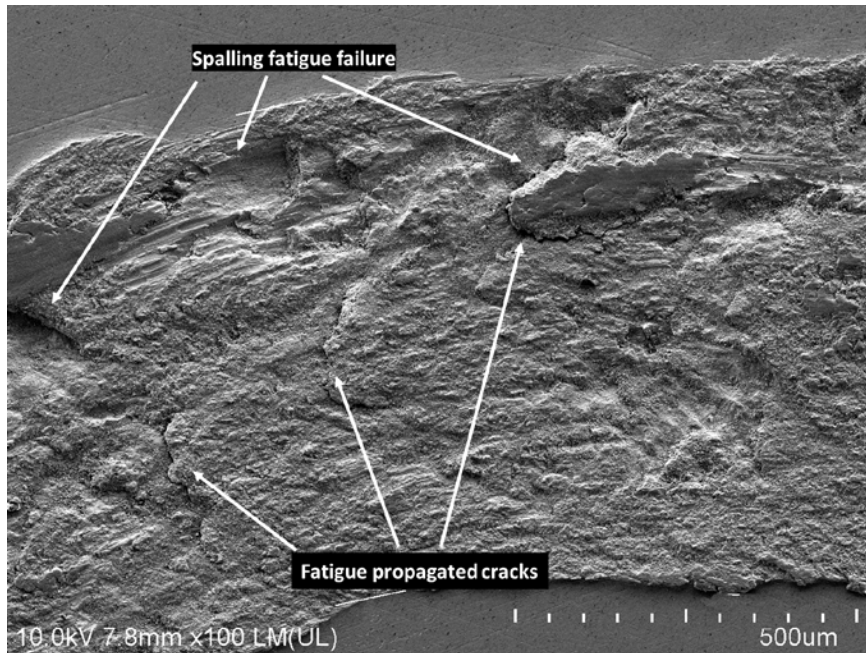
Figure 12: Development of fatigue propagated cracks in the CG niobium (initial sample): Crack initiation as a result of cyclic loading, propagation of cracks, and eventually, separation of the materials and appearance of spalling.

This difference suggests that IEAP processing of niobium enhanced the wear resistance of the materials against fatigue, at least in terms of Low Cycle Fatigue (LCF) life. As indicated in section 1, the dominance of HAGBs in SPD-induced microstructure can enhance the fatigue life of materials, providing a stable cyclic deformation response [43]. Research findings on the ECAP processing of IF steel proved that the microstructure in the processed steel with superior HAGB fractions appeared unchanged under cyclic loading. In contrast, the one with LAGB-dominated microstructure was continuously reoriented through the process and consequently, led to cyclic softening [65]. Furthermore, another study discovered that niobium is also stable at elevated-temperature fatigue tests up to the homologous temperatures of T_h= 0.32 ($T_h = \frac{T_{processing}}{T_{melting\ Point}}$; Kelvin scale) due to the high melting-point of niobium (T_m = 2477 °C), while the transition to microstructural instability in niobium starts at $0.32 < T_h < 0.34$ [61].

The last point about the experimental results that is worthwhile to mention here is the oxidative wear mechanism in the CG and UFG specimens. EDX analysis of the surface of the initial sample and IEAP-processed one after twelve passes of extrusion acknowledged the presence of a high rate of oxidation in the wear tracks in both processed and unprocessed samples (Table 2). Oxidative wear is generally known as a mild type of wear with stable conditions compared to the fluctuating conditions of severe wear conditions [57]. Niobium has a strong affinity with oxygen; dry sliding wear tests can lead to increasing the temperature and therefore intensifying the oxidation[60]. In this work, oxidative wear can be found in both cases of the CG and UFG niobium. Nonetheless, the amount of oxidation in the UFG ones is slightly higher (27-28 % oxygen vs. 23-23%) which could be due to the higher hardness resistance, and subsequently, increasing the temperature during the wear tests, and thus, increasing the oxidation rate. Detachment of nanosized wear debris observed in the processed samples with UFG microstructure (Figure 9) is an indication of a stable

wear condition in contrast to the appearance of fatigue propagated cracks in the CG niobium (Figure 12) that made the wear mechanism rough and resulted in a higher rate of wear.

As mentioned in the introduction, niobium has presented distinctive features in biomedical applications as well as nuclear and aerospace industries. Particularly with respect to implantable biomaterials, it has demonstrated high potentials thanks to its excellent corrosion resistance and biocompatibility, although suffering from relatively low yield and low ultimate strength, which could imply low fatigue resistance as well. In principle, failure in biomedical materials usually happens due to fatigue rather than yielding or overloading [48]. The present study into the impact of IEAP on the microstructural refinement of niobium uncovered clear evidence on enhancing the strength and wear resistance of the material, especially in terms of fatigue wear, while such modifications would not alter the biocompatibility of the material [43]. Therefore, it suggests the potential applications of this technique on improving the wear and fatigue performance of other metallic biomaterials that suffer from low strength and cyclic stability and paves the pathway for further research on the development of biomaterial implants.

5 Conclusion

This study, for the first time, conducted an experimental investigation into the effect of a modern severe plastic deformation technique called IEAP on grain refinement and the consequent changes in the tribological behavior of materials. IEAP is based on the indirect extrusion of materials through angular channels. A dilute niobium alloy was processed via 4, 9, and 12 passes of extrusion, and one sample was kept in initial conditions with coarse-grained (CG) microstructure as a reference. Thereafter, the microstructure and mechanical/tribological properties were investigated. The following achievements are noteworthy to summarize here:

o Results of EBSD analysis and microhardness testing confirmed that IEAP processing refined the CG microstructure towards UFG size and enhanced the hardness by increasing the pass numbers. The initial grain size of 13 μm was reduced to 500 nm, and the initial microhardness of 79 HV increased to 180 HV after twelve passes. Similarly, X-ray line profile analysis (XLPA) demonstrated a consistent increase in the dislocation density and the high angle grain boundary (HAGB) fractions in the specimens.

o Pin-on-disk experiments in dry sliding conditions revealed that IEAP processing enhanced the wear resistance of the material, particularly in terms of fatigue wear, and reduced the wear rate down to 38%. However, no remarkable change was observed in the friction coefficient.

o Investigations on the morphology of the wear tracks showed that the predominant wear mechanisms in the initial sample (CG niobium) were abrasive, fatigue, adhesive, and oxidative wear. In contrast, the processed samples (UFG niobium) showed better fatigue resistance by representing less spalling and minor cracks along with more fragmentation of small particles on the surface. By way of comparison, the wear mechanisms in the processed samples were relatively milder with less wear rate and comprised of abrasion, oxidation, and adhesion.

o Increasing the pass numbers of extrusion in IEAP, and thereby imposing further strain, increased the hardness but did not make any significant change in the wear resistance of the

material. This behavior can be explained by referring to the fact that further IEAP extrusions reduced the strain hardening capacity and decreased the ductility, thus lowering the wear resistance of the material against plastic deformation. In addition, increasing the hardness of the material after each pass of extrusion increased the material's resistance against abrasion. This resulted in a rise in the temperature of the contact surfaces during the wear test and consequently increased the rate of oxidative wear. The cumulative impact of these parameters increased the complexity of the wear and outweighed the influence of hardness increment.

o Enhancing the mechanical properties, wear resistance, and fatigue performance of UFG niobium by IEAP without altering the composition and biocompatibility suggests that this technique may offer a promising direction towards the development of other metallic biomaterials.

Conflict of interest

The authors declare that they have no known competing financial interests or personal relationships that could have appeared to influence the work reported in this paper.

References

[1]   Grill R, Gnadenberger A. Niobium as mint metal: Production–properties–processing. Int J Refract Met Hard Mater 2006;24:275–82. https://doi.org/10.1016/J.IJRMHM.2005.10.008.

[2]   Singh N, Deo MN, Roy SB. Possible influence of surface oxides on the optical response of high-purity niobium material used in the fabrication of superconducting radio frequency cavity. Nucl Instruments Methods Phys Res Sect A Accel Spectrometers, Detect Assoc Equip 2016;830:59–66. https://doi.org/10.1016/J.NIMA.2016.05.060.

[3]   Ciovati G, Dhakal P, Matalevich J, Myneni G, Schmidt A, Iversen J, et al. Mechanical properties of niobium radio-frequency cavities. Mater Sci Eng A 2015;642:117–27. https://doi.org/10.1016/J.MSEA.2015.06.095.

[4]   Kommel L. Microstructure and properties that change during hard cyclic visco-plastic deformation of bulk high purity niobium. Int J Refract Met Hard Mater 2019;79:10–7. https://doi.org/10.1016/j.ijrmhm.2018.10.009.

[5]   Wang Z, Li C, Qi J, Feng J, Cao J. Characterization of hydrogenated niobium interlayer and its application in TiAl/Ti 2 AlNb diffusion bonding. Int J Hydrogen Energy 2019;44:6929–37. https://doi.org/10.1016/j.ijhydene.2019.01.133.

[6]   Zhang X, Peng N, Liu T, Zheng R, Xia M, Yu H, et al. Review on niobium-based chalcogenides for electrochemical energy storage devices: Application and progress. Nano

Energy 2019;65:104049. https://doi.org/10.1016/j.nanoen.2019.104049.

[7]   Omranpour BS, Kommel L, Sanchez EG, Ivanisenko Y, Huot J. Enhancement of
        Hydrogen Storage in Metals by Using a New Technique in Severe Plastic Deformations.
        Key Eng Mater 2019;799:173–8.
        https://doi.org/10.4028/www.scientific.net/KEM.799.173.

[8]   Montenegro P, Gomes J, Rego R, Borille A. Potential of niobium carbide application as
        the hard phase in cutting tool substrate. Int J Refract Met Hard Mater 2018;70:116–23.
        https://doi.org/10.1016/j.ijrmhm.2017.09.017.

[9]   Pan Z, Xu F, Mathaudhu SN, Kecskes LJ, Yin WH, Zhang XY, et al. Microstructural
        evolution and mechanical properties of niobium processed by equal channel angular
        extrusion up to 24 passes. Acta Mater 2012;60:2310–23.
        https://doi.org/10.1016/j.actamat.2011.12.019.

[10]   Langdon TG. Twenty-five years of ultrafine-grained materials: Achieving exceptional
        properties through grain refinement. Acta Mater 2013;61:7035–59.
        https://doi.org/10.1016/j.actamat.2013.08.018.

[11]   Estrin Y, Vinogradov A. Extreme grain refinement by severe plastic deformation: A
        wealth of challenging science. Acta Mater 2013;61:782–817.
        https://doi.org/10.1016/j.actamat.2012.10.038.

[12]   Li JCM. Mechanical Properties of Nanocrystalline Materials. Pan Stanford Pub; 2011.
        https://doi.org/10.1002/9783527674947.ch1.

[13]   Toth LS, Gu C. Ultrafine-grain metals by severe plastic deformation. Mater Charact
        2014;92:1–14. https://doi.org/10.1016/j.matchar.2014.02.003.

[14]   Higuera-Cobos OF, Cabrera JM. Mechanical, microstructural and electrical evolution of
        commercially pure copper processed by equal channel angular extrusion. Mater Sci Eng A
        2013;571:103–14. https://doi.org/10.1016/j.msea.2013.01.076.

[15]   Need RF, Alexander DJ, Field RD, Livescu V, Papin P, Swenson CA, et al. The effects of
        equal channel angular extrusion on the mechanical and electrical properties of alumina
        dispersion-strengthened copper alloys. Mater Sci Eng A 2013;565:450–8.
        https://doi.org/10.1016/j.msea.2012.12.007.

[16]   Botcharova E, Freudenberger J, Schultz L. Mechanical and electrical properties of
        mechanically alloyed nanocrystalline Cu-Nb alloys. Acta Mater 2006;54:3333–41.
        https://doi.org/10.1016/j.actamat.2006.03.021.

[17]   Huot J. Nanocrystalline metal hydrides obtained by severe plastic deformations. Metals
        (Basel) 2012;2:22–40. https://doi.org/10.3390/met2010022.

[18]   Emami H, Edalati K, Matsuda J, Akiba E, Horita Z. Hydrogen storage performance of
        TiFe after processing by ball milling. Acta Mater 2015;88:190–5.
        https://doi.org/10.1016/j.actamat.2014.12.052.

[19]   Guo J, Zhang X, Kong D, Joo SH, Kim W, Kim HS, et al. Microstructure, Micro-
        Hardness, and Corrosion Resistance of Commercial Purity Al Processed by Hollow-Cone

High-Pressure Torsion. Adv Eng Mater 2019;21:1–7. https://doi.org/10.1002/adem.201800905.

[20]   Kim HS, Kim WJ. Enhanced corrosion resistance of ultrafine-grained AZ61 alloy containing very fine particles of Mg17Al12 phase. Corros Sci 2013;75:228–38. https://doi.org/10.1016/j.corsci.2013.05.032.

[21]   Kim HS, Yoo SJ, Ahn JW, Kim DH, Kim WJ. Ultrafine grained titanium sheets with high strength and high corrosion resistance. Mater Sci Eng A 2011;528:8479–85. https://doi.org/10.1016/j.msea.2011.07.074.

[22]   Mishnaevsky L, Levashov E, Valiev RZ, Segurado J, Sabirov I, Enikeev N, et al. Nanostructured titanium-based materials for medical implants: Modeling and development. Mater Sci Eng R Reports 2014;81:1–19. https://doi.org/10.1016/J.MSER.2014.04.002.

[23]   Bagherifard S, Ghelichi R, Khademhosseini A, Guagliano M. Cell Response to Nanocrystallized Metallic Substrates Obtained through Severe Plastic Deformation. ACS Appl Mater Interfaces 2014;6:7963–85. https://doi.org/10.1021/am501119k.

[24]   Purcek G, Karaman I, Yapici GG, Al-Maharbi M, Kuçukomeroglu T, Saray O. Enhancement in mechanical behavior and wear resistance of severe plastically deformed two-phase Zn-Al alloys. Zeitschrift fuer Met. Res. Adv. Tech., vol. 98, Carl Hanser Verlag; 2007, p. 332–8. https://doi.org/10.3139/146.101470.

[25]   Purcek G, Saray O, Kul O, Karaman I, Yapici GG, Haouaoui M, et al. Mechanical and wear properties of ultrafine-grained pure Ti produced by multi-pass equal-channel angular extrusion. Mater Sci Eng A 2009;517:97–104. https://doi.org/10.1016/j.msea.2009.03.054.

[26]   Talachi AK, Eizadjou M, Manesh HD, Janghorban K. Wear characteristics of severely deformed aluminum sheets by accumulative roll bonding (ARB) process. Mater Charact 2011;62:12–21. https://doi.org/10.1016/j.matchar.2010.10.003.

[27]   Ming Q, Yong-zhen Z, Jian-heng Y, Jun Z. Microstructure and tribological characteristics of Ti-6Al-4V alloy against GCr15 under high speed and dry sliding. Mater Sci Eng A 2006;434:71–5. https://doi.org/10.1016/j.msea.2006.07.043.

[28]   Sabirov I, Enikeev NA, Murashkin MY, Valiev RZ. Bulk Nanostructured Materials with Multifunctional Properties. 2015. https://doi.org/10.1007/978-3-319-19599-5.

[29]   Alkorta J, Pérez CJL, Popova EN, Hafok M, Pippan R, Sevillano JG. Microstructure and indentation size-effect in pure niobium subjected to SPD via ECAP and HPT. Mater. Sci. Forum, vol. 584- 586 PA, Trans Tech Publications Ltd; 2008, p. 215–20. https://doi.org/10.4028/www.scientific.net/msf.584-586.215.

[30]   Jóni B, Schafler E, Zehetbauer M, Tichy G, Ungár T. Correlation between the microstructure studied by X-ray line profile analysis and the strength of high-pressure-torsion processed Nb and Ta. Acta Mater 2013;61:632–42. https://doi.org/10.1016/j.actamat.2012.10.008.

[31]   Popov V V., Popova EN. Behavior of Nb and CuNb composites under severe plastic deformation and annealing. Mater Trans 2019;60:1209–20.

https://doi.org/10.2320/matertrans.MF201913.

[32] Popov V V., Popova EN, Stolbovskiy A V., Pilyugin VP. Thermal stability of nanocrystalline structure in niobium processed by high pressure torsion at cryogenic temperatures. Mater Sci Eng A 2011;528:1491–6. https://doi.org/10.1016/j.msea.2010.10.052.

[33] Wang CT, Gao N, Wood RJK, Langdon TG. Wear behavior of an aluminum alloy processed by equal-channel angular pressing. J Mater Sci 2011;46:123–30. https://doi.org/10.1007/s10853-010-4862-0.

[34] Avcu E. The influences of ECAP on the dry sliding wear behaviour of AA7075 aluminium alloy. Tribol Int 2017;110:173–84. https://doi.org/10.1016/j.triboint.2017.02.023.

[35] Elhefnawey M, Shuai GL, Li Z, Zhang DT, Tawfik MM, Li L. On achieving ultra-high strength and improved wear resistance in Al–Zn–Mg alloy via ECAP. Tribol Int 2021;163:107188. https://doi.org/10.1016/j.triboint.2021.107188.

[36] Omranpour B, Kommel L, Sergejev F, Ivanisenko J, Antonov M. Tailoring the microstructure and tribological properties in commercially pure aluminium processed by High Pressure Torsion Extrusion. Proc Est Acad Sci 2021;70:540–8. https://doi.org/https://doi.org/10.3176/proc.2021.4.23.

[37] Kommel L, Põdra P, Mikli V, Omranpour B. Gradient microstructure in tantalum formed under the wear track during dry sliding friction. Wear 2021;466–467:203573. https://doi.org/10.1016/j.wear.2020.203573.

[38] Fintová S, Dlhý P, Mertová K, Chlup Z, Duchek M, Procházka R, et al. Fatigue properties of UFG Ti grade 2 dental implant vs. conventionally tested smooth specimens. J Mech Behav Biomed Mater 2021;123:104715. https://doi.org/10.1016/j.jmbbm.2021.104715.

[39] Wang CT, Gao N, Gee MG, Wood RJK, Langdon TG. Processing of an ultrafine-grained titanium by high-pressure torsion: An evaluation of the wear properties with and without a TiN coating. J Mech Behav Biomed Mater 2013;17:166–75. https://doi.org/10.1016/j.jmbbm.2012.08.018.

[40] Li J, Wongsa-Ngam J, Xu J, Shan D, Guo B, Langdon TG. Wear resistance of an ultrafine-grained Cu-Zr alloy processed by equal-channel angular pressing. Wear 2015;326–327:10–9. https://doi.org/10.1016/j.wear.2014.12.022.

[41] Gao N, Wang CT, Wood RJK, Langdon TG. Tribological properties of ultrafine-grained materials processed by severe plastic deformation. J Mater Sci 2012;47:4779–97. https://doi.org/10.1007/s10853-011-6231-z.

[42] Talibouya Ba EC, Dumont MR, Martins PS, Drumond RM, da Cruz MPM, Vieira VF. Investigation of the effects of skewness Rsk and kurtosis Rku on tribological behavior in a pin-on-disc test of surfaces machined by conventional milling and turning processes. Mater Res 2021;24. https://doi.org/10.1590/1980-5373-MR-2020-0435.

[43] Niendorf T, Canadinc D, Maier HJ, Karaman I, Yapici GG. Microstructure-mechanical property relationships in ultrafine-grained NbZr. Acta Mater 2007;55:6596–605.

https://doi.org/10.1016/j.actamat.2007.08.015.

[44] Djavanroodi F, Omranpour B, Ebrahimi M, Sedighi M. Designing of ECAP parameters based on strain distribution uniformity. Prog Nat Sci Mater Int 2012;22:452–60. https://doi.org/10.1016/j.pnsc.2012.08.001.

[45] Omranpour B, Kommel L, Mikli V, Garcia E, Huot J. Nanostructure development in refractory metals: ECAP processing of Niobium and Tantalum using indirect-extrusion technique. Int J Refract Met Hard Mater 2019;79:1–9. https://doi.org/10.1016/j.ijrmhm.2018.10.018.

[46] Kommel L, Shahreza BO, Mikli V. Microstructure and physical-mechanical properties evolution of pure tantalum processed with hard cyclic viscoplastic deformation. Int J Refract Met Hard Mater 2019;83:104983. https://doi.org/10.1016/J.IJRMHM.2019.104983.

[47] Kommel L, Omranpour BS, Mikli V. Structuration of Refractory Metals Tantalum and Niobium Using Modified Equal Channel Angular Pressing Technique. Key Eng Mater 2019;799:103–8. https://doi.org/10.4028/www.scientific.net/kem.799.103.

[48] O'Brien B. Niobium Biomaterials, 2015, p. 245–72. https://doi.org/10.1007/978-3-662-46836-4_11.

[49] Djavanroodi F, Omranpour B, Sedighi M. Artificial Neural Network Modeling of ECAP Process. Mater Manuf Process 2013;28:276–81. https://doi.org/10.1080/10426914.2012.667889.

[50] Standard A. G99, Standard Test Method for Wear Testing with a Pin-on-Disk Apparatus. ASTM Int West Conshohocken, PA 2006;v:1–5.

[51] Balogh L, Ribárik G, Ungár T. Stacking faults and twin boundaries in fcc crystals determined by x-ray diffraction profile analysis. J Appl Phys 2006;100:023512. https://doi.org/10.1063/1.2216195.

[52] Ribárik G, Gubicza J, Ungár T. Correlation between strength and microstructure of ball-milled Al-Mg alloys determined by X-ray diffraction. Mater Sci Eng A 2004;387–389:343–7. https://doi.org/10.1016/j.msea.2004.01.089.

[53] Ungár T, Dragomir I, Révész Á, Borbély A. The contrast factors of dislocations in cubic crystals: The dislocation model of strain anisotropy in practice. J Appl Crystallogr 1999;32:992–1002. https://doi.org/10.1107/S0021889899009334.

[54] Zeng-Hui L, Jia-Xiang S, Zeng-Hui L, Jia-Xiang S. Elastic properties of Nb-based alloys by using the density functional theory. Chinese Phys B 2012;21:16202–016202. https://doi.org/10.1088/1674-1056/21/1/016202.

[55] Borbély A, Dragomir-Cernatescu J, Ribárik G, Ungár T, IUCr. Computer program ANIZC for the calculation of diffraction contrast factors of dislocations in elastically anisotropic cubic, hexagonal and trigonal crystals. Urn:Issn:0021-8898 2003;36:160–2. https://doi.org/10.1107/S0021889802021581.

[56] Lorenzo-Bonet E, Hernandez-Rodriguez MAL, Perez-Acosta O, De la Garza-Ramos MA,

Contreras-Hernandez G, Juarez-Hernandez A. Characterization and tribological analysis of graphite/ultra high molecular weight polyethylene nanocomposite films. Wear 2019;426–427:195–203. https://doi.org/10.1016/j.wear.2019.01.092.

[57]   Stachowiak GW, Batchelor AW. Engineering Tribology: Fourth Edition. Elsevier Inc.; 2013. https://doi.org/10.1016/C2011-0-07515-4.

[58]   Bhushan B. Principles and Applications of Tribology, Second Edition. John Wiley and Sons; 2013. https://doi.org/10.1002/9781118403020.

[59]   Popov V V., Popova EN, Stolbovskiy A V. Nanostructuring Nb by various techniques of severe plastic deformation. Mater Sci Eng A 2012;539:22–9. https://doi.org/10.1016/j.msea.2011.12.082.

[60]   Purcek G, Saray O, Rubitschek F, Niendorf T, Maier HJ, Karaman I. Effect of internal oxidation on wear behavior of ultrafine-grained Nb-Zr. Acta Mater 2011;59:7683–94. https://doi.org/10.1016/j.actamat.2011.08.028.

[61]   Rubitschek F, Niendorf T, Karaman I, Maier HJ. Microstructural stability of ultrafine-grained niobium–zirconium alloy at elevated temperatures. J Alloys Compd 2012;517:61–8. https://doi.org/10.1016/J.JALLCOM.2011.11.150.

[62]   Omranpour B, Ivanisenko Y, Kulagin R, Kommel L, Garcia Sanchez E, Nugmanov D, et al. Evolution of microstructure and hardness in aluminum processed by High Pressure Torsion Extrusion. Mater Sci Eng A 2019;762:138074. https://doi.org/10.1016/j.msea.2019.138074.

[63]   Pippan R, Scheriau S, Taylor A, Hafok M, Hohenwarter A, Bachmaier A. Saturation of fragmentation during severe plastic deformation. Annu Rev Mater Res 2010;40:319–43. https://doi.org/10.1146/annurev-matsci-070909-104445.

[64]   Garbacz H, Motyka M. Tribology. Nanocrystalline Titan., Elsevier; 2018, p. 193–208. https://doi.org/10.1016/B978-0-12-814599-9.00010-9.

[65]   Niendorf T, Canadinc D, Maier HJ, Karaman I. On the Microstructural Stability of Ultrafine-Grained Interstitial-Free Steel under Cyclic Loading. Metall Mater Trans A 2007 389 2007;38:1946–55. https://doi.org/10.1007/S11661-007-9154-1.